Draft version as of 7 Mar 2001

OH Column Abundance Over TMF 1997 - 2000

Franklin P. Mills[1], Stanley P. Sander[2], Richard P. Cageao, Vassilii Nemtchinov, Yibo Jiang, and Mark A. Allen[2],
Jet Propulsion Laboratory, California Institute of Technology, Pasadena, California

Yuk L. Yung,
California Institute of Technology, Pasadena, California

Abstract

The column abundance of OH over the Jet Propulsion Laboratory's Table Mountain Facility (TMF) has been measured regularly since Jul 1997 using the Fourier-Transform Ultraviolet Spectrometer. 4574 measurements have been made at solar zenith angles of $11 - 80$ degrees since Jul 1997. Of these, 1600 morning measurements and 1535 afternoon measurements were made between Nov 1998 and Dec 2000 at solar zenith angles $\leq 65^{\circ}$ and have fractional spectral fit uncertainties of $\leq 37\%$, with a median uncertainty of 14%. Empirical linear fits for OH column as a function of solar zenith angle have been derived. The afternoon OH column typically is larger than the morning OH column at the same solar zenith angle. After removing the first-order dependence of OH column on solar zenith angle, daily average variations in OH column over TMF were calculated. The variations observed are statistically significant, are highly correlated between morning and afternoon, and are highly correlated at all solar zenith angles $\lesssim 60^{\circ}$. The observed daily average variations in OH column are most strongly correlated with variations in O_3 and H_2O abundances at $35 - 45$ km altitude as observed near TMF by HALOE (v. 19). This qualitatively agrees with sensitivity studies made using a photochemical model with standard JPL97 chemistry. Estimated variations in OH column predicted from a linearized sensitivity analysis and the observed variations in H_2O and O_3 have a correlation coefficient of 0.47 when compared to the observed variations in OH column. The slope of the linear fit for OH column as a function of solar zenith angle is steepest in winter and shallowest in summer. This may result from the observed decrease in the O_3 column above 40 km altitude and the observed increase in the H_2O mixing ratio at $40 - 50$ km altitude in winter over TMF. The annual average OH column observed over TMF is larger than that reported over Tokyo by Iwagami et al. [1998] and smaller than that reported over Colorado [Burnett **; Canty et al. 2000] and New Mexico [Canty et al. 2000].

1. Introduction

The upper stratosphere (above 30 km altitude) contains only about 15% of the total ozone column, but ozone loss in this region affects global stratospheric temperatures and, thus, may affect stratospheric circulation [Muller et al. 1998]. In addition, this region is considered the most vulnerable to catalytic destruction by chlorine oxide radicals (ClO_x) [Muller et al. 1998], so it is the region in which the first evidence for a recovery of ozone toward preindustrial levels may be observed [Hofmann et al. 1998]. Consequently, a good understanding of the chemistry in the upper stratosphere is needed. Ozone loss in this region is dominated by reactions with chlorine oxides and odd-hydrogen species (HO_x = H + OH + HO_2), so a good understanding of both HO_x and ClO_x chemistry is needed. Current photochemical models using existing laboratory data, however, have not yielded satisfactory agreement with previous observations of OH, HO_2, and O_3 [Jucks et al. 1998, Sandor and Clancy 1998, Cónway et al. 2000]. This paper describes the first 3.5 years of measurements of OH column abundance over the Jet Propulsion Laboratory's (JPL) Table Mountain Facility (TMF) and compares these measurements to available O_3 and H_2O profiles near TMF with the aid of a photochemical model.

Profiles for OH in the stratosphere and mesosphere have been measured by several groups since the early 1980s [Canty et al. 2000]. Three recent studies [Jucks et al. 1998, Conway et al. 2000, Summers et al. 1997] have been particularly important because OH profiles were measured simultaneously with those of other relevant species (O_3, H_2O, and/or HO_2). These three studies concluded that present photochemical models do not seem to accurately capture the actual HO_x chemistry in the stratosphere and mesosphere. All three studies, however, suffer from the limited duration of their measurements, so they have sampled only a small fraction of the range of conditions that may exist in the stratosphere and mesosphere.

One additional tool that may be used for analyzing the daytime photochemistry in the upper stratosphere and mesosphere is column- integrated measurements of OH abundance. The measured peak abundance of OH is at 40 – 45 km altitude with a rapid decrease toward lower altitudes and a slower decrease toward higher altitudes [Conway et al. 2000, Canty et al. 2000]. As a result, column integrated OH abundances should be most sensitive to changes in the photochemical state of the 30 – 60 km altitude region. At these altitudes, the calculated photochemical lifetime for OH is less than 300 seconds, so the changes in OH column abundance on longer timescales that have been observed [e.g., Burnett et al. 1989, Iwagami et al. 1998, this work] should be controlled by variations in the abundances and photolysis rates of the reservoir species from which OH is derived: O_3 and H_2O. Thus, coordinated observations of OH, O_3, and H_2O should provide good observational constraints on the photochemistry in the upper stratosphere and mesosphere.

Regular measurements of OH column abundance have been made over Fritz Peak, Colorado, since 1977 [e.g., Burnett and Minschwaner 1998 and references therein]. OH column abundance was also measured over Tokyo, Japan, in 1992 - 1995 [Iwagami et al. 1998]. Long-term measurement records, such as these, are necessary for determining correlations between OH column abundance and climatic or dynamic changes in the upper stratosphere and mesosphere. The Fritz Peak data set has a number of interesting features. (a) A diurnal asymmetry in the OH column abundance that changes with season [Burnett and Burnett 1984]. (b) A correlation of OH column abundance with solar cycle [Burnett et al. 1989]. (c) Interannual changes in the seasonal variation of OH column abundance [Burnett and Minschwaner 1998; Burnett and Burnett 1996]. These and other features of this data set have been difficult to explain in terms of known photochemical processes. Due to a lack of corroborating data, it is not clear which of the observed features are artifacts and which imply that major changes are needed in current photochemical models. The Tokyo data set is much shorter in duration, but the diurnal and seasonal variations in the Tokyo data set are generally smaller? in amplitude than in the Fritz Peak data set. In addition, the absolute OH column abundances for the 1992 - 1995 period for the two sites differ from each other and from model predictions by larger amounts than the mutual uncertainties.

The temporal variations in the FPO and Tokyo data sets have not been satisfactorily explained in terms of relevant geophysical parameters, and, partly due to the difficulties involved in interpreting column measurements, neither data set has received significant attention from outside modeling programs. In particular, no attempt has been published to see if intraannual variations in O_3 and H_2O in the upper stratosphere and mesosphere are correlated with and

can explain observed intraannual variations in OH column. This will be examined in this paper using the OH column abundance measurements over TMF and available H_2O and O_3 measurements from near TMF.

2. Observations

Since July 1997, OH column abundance has been measured regularly over the Jet Propulsion Laboratory's (JPL) Table Mountain Facility (TMF) using the Fourier-Transform Ultraviolet Spectrometer (FTUVS) [Cageao et al. 2001]. FTUVS collects spectra of the Sun from the ground with unapodized resolving power near 500,000 by viewing the east and west limbs of the Sun, alternately, for 15 minutes each. The Doppler-shift induced by the rotation of the Sun shifts the solar Fraunhofer lines relative to the telluric OH lines. Consequently, in the ideal situation, a properly shifted ratio of a pair of east and west limb spectra will remove the solar Fraunhofer lines and leave only features due to the telluric gases that are along the line of sight to the Sun. The OH absorption features in the ratio spectra are fit with a calculated ratio spectrum in a linear least squares manner to determine the line of sight OH abundance. The line of sight abundance is converted to a vertical column abundance by dividing by the secant of the solar zenith angle. The OH absorption lines that are observed in the near UV are optically thin unlike OH emission measurements in the far infrared [Pickett and Peterson 1993], so the ground-based near UV measurements are sensitive to the entire OH column. No information on the vertical profile of OH is presently derived from the near UV column measurements because (a) the abundance of OH varies throughout the day at any given altitude and (b) the line width is Doppler-limited above the stratopause. Further information on the measurement technique may be found in Cageao et al. [2001].

Measurements, typically, are made throughout a day for solar zenith angles less than 80 degrees. Figure 1 shows the approximate range of solar zenith angles that can be observed at TMF throughout the year and the solar zenith angles at which measurements have been made on each morning since 1 July 1997. The afternoon data coverage since January 1998 is similar. The collecting optics that bring sunlight to FTUVS were upgraded in September - December 1999 to improve the signal-to-noise ratio of the spectra.

Seven OH lines are routinely observed by FTUVS: $P_1(3)$ at 32340.585 cm^{-1}, $P_1(2)$ at 32390.885 cm^{-1}, $P_1(1)$ at 32440.573 cm^{-1}, $Q_1(3)$ at 32441.817 cm^{-1}, $Q_1(2)$ at 32458.027 cm^{-1}, and a blend of the $Q_1(1)$ and $QP_{21}(1)$ lines at 32474.214 and 32474.553 cm^{-1}, respectively. The most internally consistent results are obtained for the $P_1(1)$ line which was used by the Burnett and Iwagami groups, so this paper will focus on analysis of the results from the $P_1(1)$ line. Cageao et al. [2001] found that the primary source for uncertainty in the measured OH column abundance was the spectral fit. The total 1σ random uncertainty from all other sources was estimated by Cageao et al. [2001] to be 7% and the total 1σ systematic uncertainty from all sources was estimated by Cageao et al. [2001] to be 6%. Figure 2 gives a histogram of the calculated fit uncertainties for the $P_1(1)$ line for data collected from November 1998 to December 2000. A total of 3720 OH column abundance measurements were made in that two year two month period. Satisfactory spectral fits were derived for 3695 measurements and 3560 have fractional spectral fit uncertainties that are less than 37%. 37% is the smallest fractional uncertainty where a local minimum in the histogram is below five. The median spectral fit uncertainty for the measurements was 14%.

3. Results

Figure 3 provides an overview of the entire set of morning data for OH column abundance over TMF. The afternoon data are similar. The projection of the data on the xy-plane shows that the colors have been specified based on the solar zenith angle of the measurements. The sinusoidal envelope around the main scatter plot of the data is the three-dimensional projection of the minimum solar zenith angle curve shown in Figure 1. The gradation in colors from light green to dark green shows that OH column abundance generally increases with decreasing solar zenith angle. This is shown more clearly in the projection of the data on the xz-plane. The mixture of colors in the main scatter plot indicates that OH column abundance is not a monotonic function of either day of year or solar zenith angle (or both). A large component of the scatter, however, does appear to be due to seasonal changes in the relationship between solar zenith angle and OH column abundance. The remainder of the scatter could be due to real, stochastic fluctuations in the atmosphere or the presence of time-variable thin clouds or aerosols. It also is possible that there are systematic instrumental or analysis effects that have not yet been isolated. However, the

temporal variations in OH column abundance that are reported here for the $P_1(1)$ line generally are also observed in the other OH lines that are monitored by FTUVS.

Figure 3 shows that OH column abundance is a strong function of solar zenith angle. Solar zenith angle, in turn, is a function of both time of day and solar declination angle. This solar zenith angle dependence must be removed in order to look for smaller-amplitude intraannual variations of the OH column abundance that are due to changes in other geophysical parameters, such as changes in H_2O or O_3 abundances. To do this, an empirical, linear least-squares fit was calculated for the measured OH column abundance as a function of solar zenith angle, Figure 4. All measured data from November 1998 to December 2000 with fractional spectral fit uncertainty less than 37% and solar zenith angle less than 65° were included in determining these linear fits. The rationale for selecting 37% as the maximum fractional fit uncertainty is in Section 2. Only data at solar zenith angles less than 65° were used because the measurements at solar zenith angles $\gtrsim 70^\circ$ have significantly larger fractional fit uncertainties. The best fit curves and the uncertainties on the best fit were calculated using a singular value decomposition technique [Press et al. 1989, chapter 14] in which the measurements were weighted by the inverse of their total random uncertainty [Bevington 1969?]. The uncertainties included in these calculations were the RMS sum of the random uncertainties from Cageao et al. [2001] and the spectral fit uncertainties (Figure 2). For comparison, the mean OH column abundance was calculated for each two degree solar zenith angle bin and these mean values are plotted in Figure 4 along with the uncertainty on the mean value for each bin. The mean and uncertainty on the mean were calculated by weighting the measurements by the inverse of their total random uncertainty [Bevington 1969?]. The 1σ scatter that is plotted for each solar zenith angle bin illustrates the range of values that have been measured for each bin. The full range of the scatter can be seen in Figure 3.

The empirical best-fit lines from Figure 4 were used as a first-order estimate for removing the dependence of OH column abundance on solar zenith angle. The measured OH column abundances were divided by the "expected" OH column abundance to derive normalized OH column abundances. Inspection of the normalized OH column abundances showed no obvious biases as a function of solar zenith angle, so the normalized OH column abundances appear to adequately capture the observed variability in the measured OH column abundances. The normalized OH column abundances for each day were averaged to obtain the values shown in Figure 5. Variability on time scales of days to months is evident and much of the variability is statistically significant because it is larger than the uncertainties.

The daily averages plotted in Figure 5 indicate OH column abundance over TMF may have been generally increasing over the time from 1997 to 2000. The measurement time period, however, is too short and the amplitude of any interannual trend is too small to provide a definitive conclusion at this time. The typical peak-to-peak amplitude of the intraannual variations in OH column abundance over TMF is $\sim 30\%$. The $> 40\%$ change in OH column for a one week period in April 2000 may be connected to solar activity and will be discussed in a future publication.

The variations in the morning and afternoon daily averages (Figure 5) are highly correlated, Figure 6. The Pearson linear correlation coefficient between the morning and afternoon daily averages is 0.87 with a two-sided statistical significance level of smaller than 0.1%. The Spearman nonparametric correlation coefficient is 0.86 with a two-sided significance level smaller than 0.1%. The Pearson and Spearman correlation coefficients and statistical significance levels were computed using the methodology described in Press et al. [1989], Chapter 13. The Pearson test assumes the variables jointly form a binormal distribution, and a Pearson correlation coefficient of 0.87 implies that 76% of the observed variation in the afternoon daily average can be explained by the observed variation in the morning daily average. A higher degree of correlation is unlikely due to the presence of measurement uncertainty. The Spearman test is a more robust, rank-order correlation that does not require a binormal distribution. The two-sided significance levels were computed using the Student's t-distribution, so that the significance levels are meaningful even when the number of data is not large. Autocorrelations were calculated for the Jan 1998 to Dec 2000 morning and afternoon daily average data at time lags of $1-183$ days. "Strong" autocorrelations were found at time lags of 1 and 47 days. Both the morning and afternoon autocorrelations had Pearson and Spearman correlation coefficients > 0.6 and two-sided significance levels smaller than 0.1%. Due to the irregular measurement intervals, the degree to which the strong autocorrelation at 47 days is the result of geophysical phenomena is not clear.

Normalized data at different solar zenith angles also are highly correlated, reinforcing the significance of the variations shown in Figure 5. Daily averages of the normalized OH data were computed for 20 degree ranges of solar zenth angle ($10-30$,$20-40$,...,$50-70$), then all unique cross correlations were calculated. The two-sided significance level for all cross correlations was smaller than 0.1%. Morning and afternoon were computed separately. The smallest correlation coefficient for solar zenith angles $\leq 60^{\circ}$ was 0.79. The smallest correlation coefficient using the $50-70^{\circ}$ range was 0.67. The smallest correlation coefficient between the $10-65^{\circ}$ daily average and the 20° daily averages was 0.87. The worst correlations were always for morning data at large solar zenith angles.

Separate linear fits were calculated (Figure 4) for morning and afternoon because there is a clear and consistent throughout the year asymmetry between OH column abundances in the morning and afternoon, Figure 7 and Table 3. The fits for September, October, and December are the most uncertain due to the limited number of measurements in those three months. Excluding those three months, the steepest slopes for OH column as a function of solar zenith angle are found in the winter over TMF.

Table 1. Monthly empirical fits for OH column abundance over TMF

Month[1]	SZA range[2]	Morning			Afternoon		
		Intercept[3]	Slope[4]	# Data[5]	Intercept[3]	Slope[4]	# Data[5]
1	$52.4-64.9$	9.13 ± 1.25	-8.31 ± 2.13	111	8.35 ± 1.27	-6.41 ± 2.17	121
2	$43.5-65.0$	8.38 ± 0.65	-7.13 ± 1.20	145	7.80 ± 0.67	-5.42 ± 1.23	148
3	$30.5-65.0$	7.46 ± 0.28	-5.76 ± 0.60	182	6.75 ± 0.29	-3.58 ± 0.60	183
4	$20.4-65.0$	7.68 ± 0.23	-6.13 ± 0.52	155	6.43 ± 0.24	-3.16 ± 0.53	142
5	$12.4-64.2$	7.21 ± 0.18	-5.22 ± 0.42	150	7.19 ± 0.20	-3.42 ± 0.48	141
6	$11.4-64.9$	8.35 ± 0.15	-6.37 ± 0.34	223	8.10 ± 0.18	-4.58 ± 0.43	185
7	$11.4-64.9$	8.18 ± 0.17	-6.16 ± 0.40	152	7.70 ± 0.19	-4.03 ± 0.44	146
8	$15.9-65.0$	8.20 ± 0.17	-6.29 ± 0.39	206	7.65 ± 0.17	-3.90 ± 0.40	207
9	$27.8-64.8$	9.24 ± 0.41	-7.99 ± 0.86	71	8.13 ± 0.45	-4.79 ± 0.92	63
10	$38.8-62.7$	9.66 ± 1.48	-8.31 ± 2.91	13	10.20 ± 1.67	-8.03 ± 3.30	13
11	$50.0-65.0$	10.10 ± 0.78	-10.10 ± 1.35	163	7.41 ± 0.74	-4.75 ± 1.29	171
12	$56.7-64.8$	7.11 ± 2.75	-5.49 ± 4.59	29	5.26 ± 4.29	-1.82 ± 7.11	15

[1]Data used in fit was collected in Nov 1998, Jan - Aug 1999, and Jan - Dec 2000.

[2]Range of solar zenith angles used

[3]10^{13} cm^{-2}

[4]10^{11} cm^{-2} per degree

[5]Number of OH column abundance measurements used in fit

4. Other OH Column Measurements

As shown in Figure 4, the annual average OH column abundance over TMF in Nov 1998 - Dec 2000 is smaller at all solar zenith angles than that reported over Fritz Peak Observatory (FPO) in Colorado for 1980 – 1990 and for 1996. The annual average over TMF is also smaller than that reported over Socorro, New Mexico, for 1996, but the annual average over TMF is larger than that derived from the reported monthly averages over Tokyo for 1992 - 1995. The small number of OH column abundance measurements published by Notholt et al. [1997] and Pickett and Peterson [1996] are not included in Figure 4 due to the limited extent of those data sets. All of the annual average data sets indicate afternoon OH column abundances are typically larger than morning OH column abundances at the same solar zenith angle.

The derived annual average over Tokyo is within the one standard deviation scatter of data collected over TMF at most solar zenith angles. The scatter for the monthly average OH column measurements over Tokyo about the annual average is comparable to the scatter about the annual average for TMF. The results from our model sensitivity analyses (Section 5), the observed interannual variations in H_2O ($\lesssim$ 2% per year increase) and O_3 (< 1% change per year) at midlatitudes for 30 – 50 km altitude [Randel et al. 1999; Evans et al. 1999], and the observed variability within latitudinal bins for O_3 ($\sim$ 5%) at midlatitudes for 30 – 40 km altitude [Wang et al. 1999] suggest that the differences between the TMF and Tokyo annual average OH column are sufficiently small that the differences might be due to geophysical variance. The differences between the annual average OH column over TMF and those measured over FPO and New Mexico are larger than what would be expected due to observed geophysical variability in H_2O and O_3 at most solar zenith angles. For the same reasons, the largest interannual variations in OH column reported over FPO [Burnett et al. 1989?; Burnett and Minschwaner 1998] do not seem to be explainable in terms of the observed variations in H_2O and O_3. Although a possible trend of increasing OH column is visually evident in Figure 5, the TMF measurement record is not sufficiently long to reliably detect small interannual variations. No obvious evidence exists in the 1997 – 2000 TMF data for large interannual variations.

Normalized intraannual variations have been reported for OH column abundances over FPO and Tokyo. Due to the normalization, these variations may be affected less by any systematic instrumental differences between the different sites (which use different techniques and/or instrumentation). The amplitude of the intrannual variations observed over FPO in 1980 – 1995 (peak-to-peak $\sim$ 30 – 35% [Burnett et al. 1989; Burnett and Burnett 1996; Burnett and Minschwaner 1998]) appears to be comparable to that observed over TMF in 1998 - 2000 ($\sim$ 30% peak-to-peak). Similarly, the peak-to-peak intraannual variations in OH column abundance "near-noon" over TMF for 1998 – 1999 are to be similar to those reported by Iwagami et al. [1998] for the OH column abundance over Tokyo in 1992 – 1995.

Comparisons using very small size data sets between the single solar-absorption spectrum method and the solar limb ratio method found no significant difference in the derived OH column [Notholt et al. 1997; Minschwaner, Personal Communication, 1999]. This suggests that the differences in OH column abundance derived by each group may not be due to the differing observational and analysis techniques, but detailed cross comparisons are needed. Further analysis, including careful modeling of the conditions appropriate to each location, also is required. Due to the different time periods, locations, instruments, and analysis techniques, further comparisons among the four data sets are deferred to a subsequent publication.

5. Model Sensitivity Analysis

A series of sensitivity calculations was made using the Caltech/JPL one-dimensional photochemical model [Allen et al. 1981] to assess what geophysical parameters are most likely to be responsible for the variations shown in Figure 5. The results are summarized in Table 5 and in Figure 9. The baseline photochemical model was initialized with species concentrations measured near 30° N in Mar 1985 by the Atmospheric Trace Molecule Spectroscopy (ATMOS) Experiment [Allen and Delitsky 1991], run to a diurnally-averaged steady-state condition with vertical transport via eddy diffusion, and then run in a diurnally-varying mode without vertical transport until the modelled diurnal cycle for OH at all altitudes between 25 and 80 km was repeated to within 1%. For the sensitivity calculations, the diurnally-averaged steady-state concentrations at 25 – 80 km altitude of H_2O, CH_4, NO_y, Cl_y, and CO were perturbed

by ±25%. The model was then run in diurnally-varying mode until the modelled diurnal cycle for OH at all altitudes between 25 and 80 km was repeated to within 1%. The calculated response OH column response given in Table 5 is the maximum difference in calculated OH column between the baseline model calculation and the modified calculation, scaled linearly to match the maximum expected change that is expected for these species. The maximum expected changes are based on the analyses in **refs** for the 1992 – 1997 time period. All model calculations used the recommended values from DeMore et al. [1997]. The changes recommended in DeMore et al. [2000] are not believed to be significant for the sensitivity calculations. Transmission and absorption in the O_2 Schumann-Runge Band was calculated using the Allen and Frederick [1982] parameterization as updated by Froidevaux et al. [1985?]. The solar fluxes used were taken from Mount and Rottman [1983] and WMO [1981].

The most important result from the sensitivity calculations in Table 5 is that a photochemical model using the currently assessed best parameters predicts that OH column abundance primarily is sensitive to the abundance of H_2O. This also means that OH column abundance should be sensitive to local changes in O_3 abundances because the primary mechanism for producing OH below 60 km altitude in the model is the reaction

$$O(^1D) + H_2O \rightarrow 2OH.$$

The sensitivity to $O(^1D)$ production was confirmed by examining, separately, the sensitivity of the OH column abundance to production of $O(^1D)$ and $O(^1P)$ from photolysis of O_3. 25% changes in the rates of the photolysis reactions producing $O(^1P)$ led to negligible changes in the OH column abundance, while 25% changes in the rates of the photolysis reactions producing $O(^1D)$ gave changes in the OH column abundance that are comparable to those in Table 5 for changes in H_2O abundance.

The altitude and local time dependence of the sensitivity of OH column abundance to changes in H_2O concentration was tested in a similar manner with the results shown in Figure 9. As expected, the OH column is most sensitive to changes in H_2O concentrations at 35 – 50 km altitude.

Table 2. Sensitivity of Modeled OH Column to Variations in Geophysical Parameters

Parameter[1]	Expected[2] Variation	Calculated[3] Response
Solar Flux	Min to Max	10%
H_2O	±25%	±10%
Surface Albedo[4]	0 – 1.0	8%
CH_4	±25%	±1%
NO_y	±5%	±0.5%
Cl_y	±10%	±0.25%
CO	±5%	±0.1%

[1]Parameter that was varied in the sensitivity calculation. Species abundances were changed at 25 – 80 km altitude.

[2]Expected maximum range of variability for the parameter.

[3]Change induced in OH column abundance.

[4]Primary effect is on $O(^1D)$ production via photolysis of O_3

6. Discussion

Four potential sources are available for measurements of H_2O and O_3 concentrations near TMF. Colocated at TMF are an ozone LIDAR [ref??] and a microwave spectrometer for profiling mesospheric H_2O [ref??]. Neither, however, provides good quality data over the full 30 – 70 km altitude range that is relevant for analysis of the OH column measurements. The Microwave Limb Sounder (MLS) on the Upper Atmosphere Research Satellite (UARS) has been operated only sporadically since 1997. The Halogen Occultation Experiment (HALOE) on UARS measured profiles of O_3 and H_2O within 10° longitude and 5° latitude of TMF on the dates shown in Figure 10.

Same day observations by HALOE near TMF and FTUVS occurred on only four days between Jul 1997 and Dec 2000. Observations separated by no more than one day occurred on 35 occasions, and observations separated by no more than two days occurred on 82 occasions. Figure 11 shows the best correlations that were found between variations in OH and HALOE H_2O and O_3 as a function of altitude. Figure 12 shows scatter plots for the correlations at selected altitudes. The altitudes that have the best correlations are within the range where the photochemical model predicts the OH column should have the greatest sensitivity to H_2O and O_3, Figure 9. This qualitatively confirms predictions from standard photochemical models.

Initial comparisons between the predicted variations in OH column abundance and the observed are shown in Figure 13. The predicted variations were calculated based on a simplified algebraic expression relating variations in OH concentration at $30-60$ km altitude to variations in the concentrations of H_2O and O_3,

$$\Delta([OH]) = \kappa \times \Delta(\{O_3 overcolumn\}^2[O_3][H_2O]),$$

where [a] = concentration of a, κ is a constant of proportionality that varies with altitude (and time of day and day of year), and $\{O_3$ overcolumn$\}$ = column abundance of O_3 above the specified altitude. The constant of proportionality used in computing the predicted variations of the OH column were the noontime weighting functions from Figure 9. Figure 13 shows significant scatter, but a general correlation between the predicted and observed OH column values is evident. The Pearson correlation coefficient is 0.47 with a two-sided significance level of **. Comparisons between full model calculations and the observed OH column variations will be discussed in a subsequent publication.

Figure 10 and the seasonal variations of H_2O observed over TMF by Nedoluha et al. [2000] provide a possible explanation for the seasonal variations shown in Figure 7. The O_3 column above 40 km altitude is smallest during winter months which should shift production of $O(^1D)$ toward lower altitudes and H_2O mixing ratios at $40-50$ km altitude were largest in winter for $1993-1997$. Both of these seasonal changes should make production of OH more sensitive to changes in solar zenith angle in winter months, as is observed.

7. Acknowledgements

The research described in this paper was performed at the Jet Propulsion Laboratory, California Institute of Technology, and jointly sponsored by Caltech and the National Aeronautics and Space Administration.

Figure 1. Conditions for which OH column abundance has been measured over JPL's TMF in the morning. Each symbol represents one column measurement. The solid line is the approximate minimum solar zenith angle that may be observed from TMF (neglecting the Earth's orbital eccentricity). The dates along the abscissa are in month/day format. (a) 1997. (b) 1998. (c) 1999. (d) 2000.

Figure 2. Histogram of the fractional uncertainties for the spectral fit to measured ratio spectra ($\Delta column/column$) for the $P_1(1)$ line of OH as observed over TMF. 3695 measurements were included in the histogram and 3560 have fractional fit uncertainties smaller than 37%. The width of each bin in the histogram is 0.01.

Figure 3. Morning OH column abundance measured over JPL's TMF from 1 July 1997 to 31 Dec 2000 as a function of date and solar zenith angle. The main plot gives a three-dimensional scatter plot of the measurements. Each color was used for a 10° wide range of solar zenith angles as shown by the projection on the xy-plane. The xz-plane also shows a projection of all measurements onto that plane. The points in the main scatter plot are shown as asterisks and the points in the two planar projections are shown as squares.

Figure 4. OH column abundance for November 1998 to December 2000 over TMF as a function of solar zenith angle. The solid line is the best fit line as calculated using a singular value decomposition technique for a least-squares fit weighted inversely by the total random uncertainty for each measurement. The dashed line is the one standard deviation uncertainty on the best fit considering only the random uncertainty on the measurements. The dotted line is the one standard deviation uncertainty on the best fit considering both the random and systematic uncertainties on the measurements. The symbol $\times$ specifies the mean value for all OH column abundances within the two degree solar zenith angle bin centered on that solar zenith angle. The mean value and the one standard deviation on the mean were calculated by weighting the measurements by the inverse of their total random uncertainty. The symbol + marks the 1σ scatter about the mean value for each solar zenith angle bin. (a) Morning data. The best fit line has intercept of $8.07(\pm 0.07) \times 10^{13}$ cm^{-2} and slope of $-6.46(\pm 0.14) \times 10^{11}$ cm^{-2}/degree. (b) Afternoon data. The best fit line has intercept of $7.77(\pm 0.07) \times 10^{13}$ cm^{-2} and slope of $-5.08(\pm 0.15) \times 10^{11}$ cm^{-2}/degree.

Figure 5. Daily average normalized OH column abundance over TMF. Measured OH column abundances (Figure 3) were divided by the "expected" OH column abundance (Figure 4) then all measurements collected on a single day were averaged. The mean and one standard deviation uncertainty on the mean for each day were calculated by using the inverse of the total random uncertainty as a weighting factor for each measurement [Bevington 1969?]. Only data collected at solar zenith angles $\leq 65^{\circ}$ were used. For data collected after October 1998, only data with fractional spectral fit uncertainty less than 37% were used. For measurements prior to November 1998, spectral fit uncertainties are not yet available, so the median uncertainty from the more recent measurements was used for all of the earlier measurements. The uncertainty on the normalization fit (Figure 4) was not included. The numerical value of one has been subtracted from each of the daily averages to give values that are centered around zero. Consequently, the plotted values represent the fractional deviation from the empirical best fit curves in Figure 4. (a) Morning data. (b) Afternoon data.

Figure 6. Scatter plot of normalized daily averages for morning versus afternoon OH column abundance measurements. The data from Figure 5 are shown.

Figure 7. Slopes for best fit lines describing OH column abundance over TMF as a function of solar zenith angle for each month. The morning (squares) and afternoon (asterisks) slopes and uncertainties are from Table 3. Data from Nov 1998 to Dec 2000 at solar zenith angles $\leq 65^{\circ}$ with fractional spectra fit uncertainty $\leq 37\%$ were used in the calculations. The uncertainties on the slope are largest in winter due to two factors: (1) the smaller number of measurements in some months and (2) the smaller range of solar zenith angles that are sampled. The best fit afternoon slopes are less steep than the morning slopes for all months and the steepest slopes are found in the winter over TMF.

Figure 8. Comparison of the annual average OH column abundance over four different sites and four different time periods. The solid line is the best fit line for the OH column over TMF for Nov 1998 - Dec 2000. The dotted line is the best fit line for the OH column over Tokyo for May 1992 - Apr 1995. The best fit line was calculated by fitting a line in a weighted least-squares manner to the monthly average OH column abundances reported by Iwagami et al. [1998] for solar zenith angles $\leq 65^{\circ}$. The morning fit is $(6.50 \pm 0.14) \times 10^{13} - SZA * (4.56 \pm 0.30) \times 10^{11}$ molecules/cm^2. The afternoon fit is $(6.36 \pm 0.12) \times 10^{13} - SZA * (4.14 \pm 0.26) \times 10^{11}$ molecules/cm^2. The dash-dot line is the annual average over FPO for 1980 – 1990 [Burnett and Burnett 1996]. The squares mark the annual average over FPO for 1996 [Canty et al. 2000]. The triangles mark the annual average over Socorro, New Mexico, for 1996 [Canty et al. 2000]. The plus signs indicate the range of scatter observed within each two degree solar zenith angle bin for the OH column over TMF for Nov 1998 - Dec 2000. (a) Morning data. (b) Afternoon data.

Figure 9. Sensitivity of modelled OH column abundance to changes in H_2O concentrations as a function of altitude and solar zenith angle (local time). The contoured values are the percentage change in the OH column abundance that would result from a 1% change in the H_2O concentration over a one kilometer thick layer centered at the plotted altitude. Hence, the units for the contoured values are (percent change in OH column) per km per (percent change in local H_2O concentration).

Figure 10. Daily average O_3 overcolumn above 40 km altitude near TMF. Derived by averaging all HALOE v. 19 O_3 profiles that were collected on a single day within 5° latitude and 10° longitude of TMF. Triangles indicate sunset profiles and asterisks indicate sunrise profiles.

Figure 11. Best Pearson correlation coefficients for covariations in HALOE H_2O, O_3, and H_2O * O_3 as a function of altitude versus TMF OH column. Squares indicate correlations with H_2O, asterisks indicate correlations with O_3, triangles indicate correlations with H_2O * O_3 at sunrise, and diamonds indicate correlations with H_2O * O_3 at sunset. Correlation coefficients were calculated at three km intervals from 25 to 79 km altitude. Those for which the two-sided significance level was smaller than 5% are plotted.

Figure 12. Covariations of HALOE H_2O, O_3, and H_2O * O_3 at 46, 40, and 40 km altitude, respectively, versus TMF OH column. Symbol key is the same as in Figure 11.

Figure 13. Covariations of predicted and observed OH column variations. See text for details of the method used to estimate the predicted variations. Squares indicate morning OH column over TMF versus HALOE sunrise. Asterisks indicate afternoon OH column over TMF versus HALOE sunrise. Triangles indicate morning OH column over TMF versus HALOE sunset. Diamonds indicate afternoon OH column over TMF versus HALOE sunset.

Figure 1

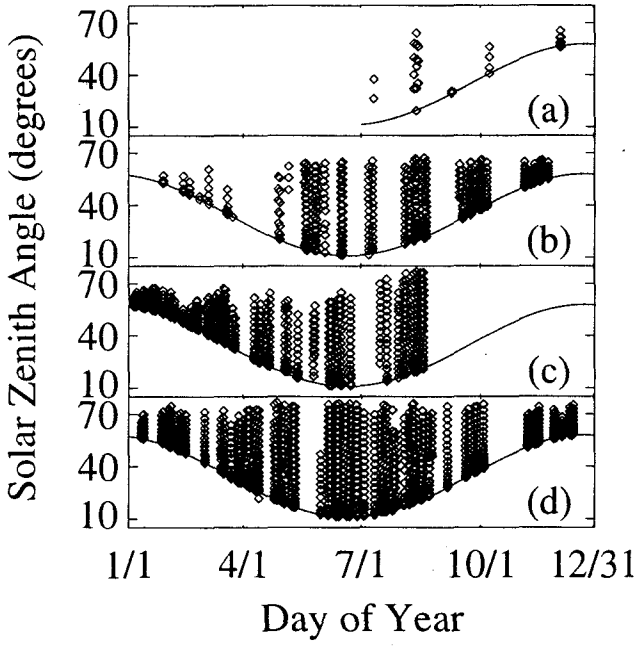
Solar Zenith Angle (degrees)
70
40
10
(a)
(b)
(c)
(d)
1/1
4/1
7/1
10/1
12/31
Day of Year

Figure 2

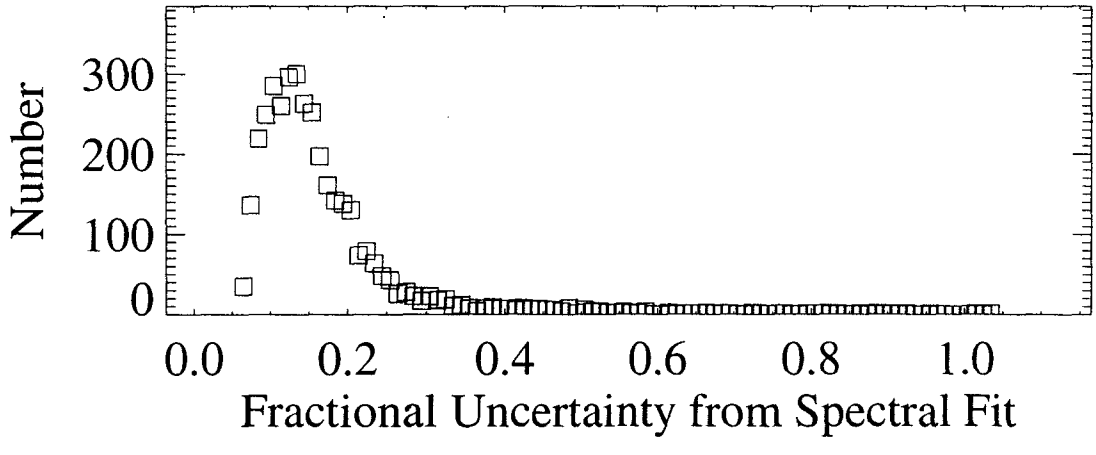
Number
300
200
100
0
0.0
0.2
0.4
0.6
0.8
1.0
Fractional Uncertainty from Spectral Fit

Figure 3

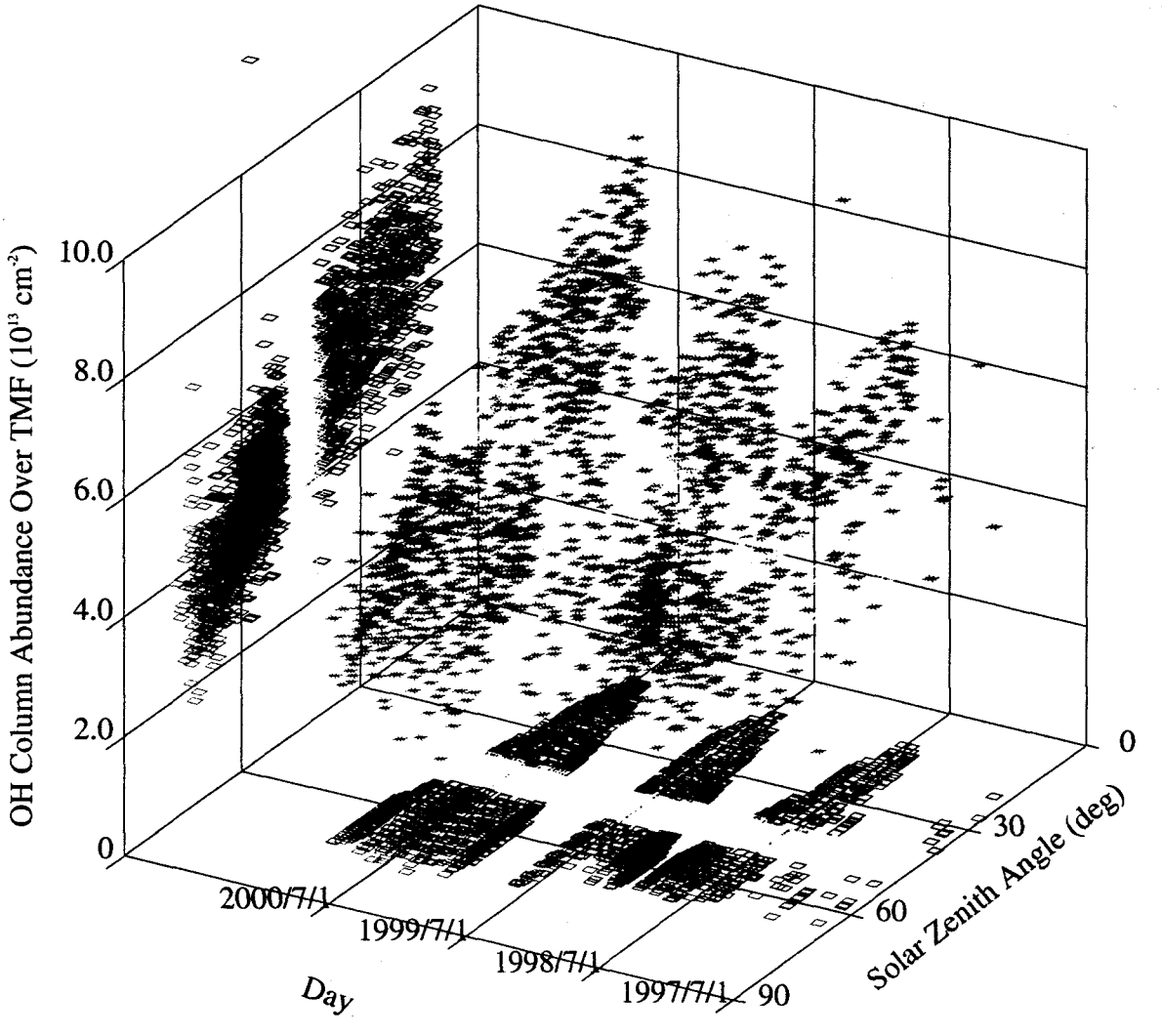
OH Column Abundance Over TMF (10^{13} cm^{-2})
10.0
8.0
6.0
4.0
2.0
0
2000/7/1
1999/7/1
1998/7/1
1997/7/1
Day
0
30
60
90
Solar Zenith Angle (deg)

Figure 4

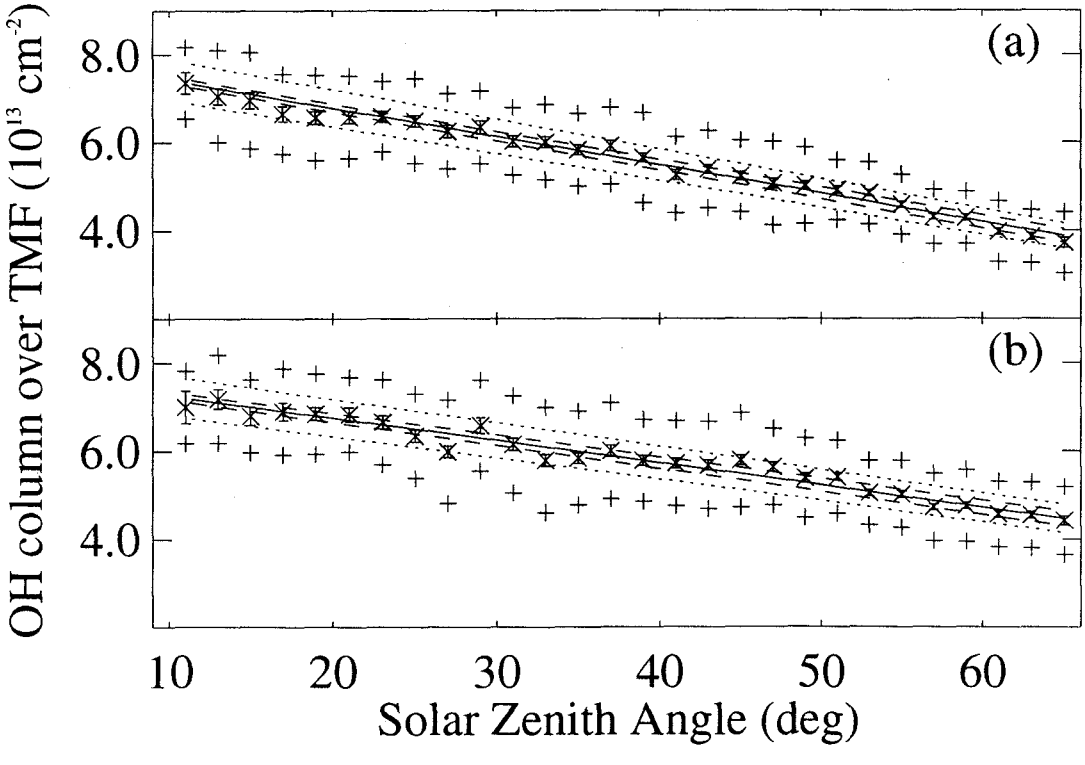
OH column over TMF (10^{13} cm^{-2})
8.0
6.0
4.0
(a)
8.0
6.0
4.0
(b)
10
20
30
40
50
60
Solar Zenith Angle (deg)

Figure 5

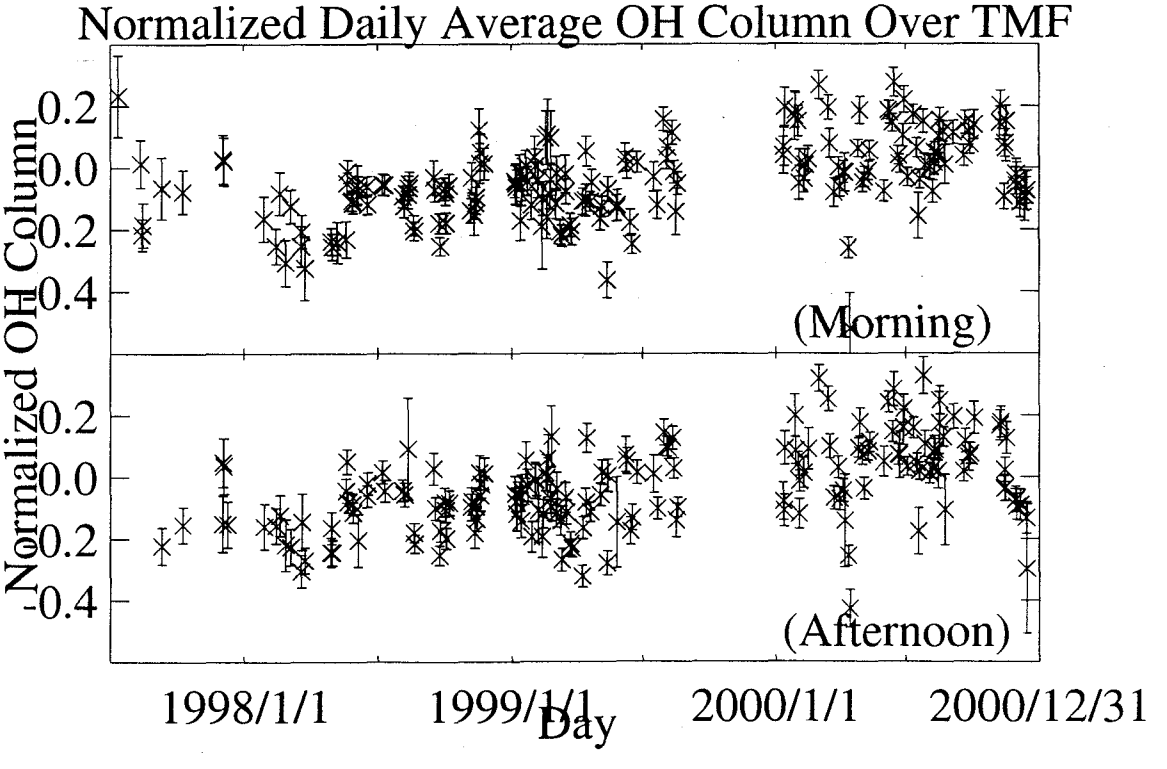
Normalized Daily Average OH Column Over TMF
Normalized OH Column
0.2
0.0
-0.2
-0.4
(Morning)
(Afternoon)
1998/1/1
1999/1/1
2000/1/1
2000/12/31
Day

Figure 6

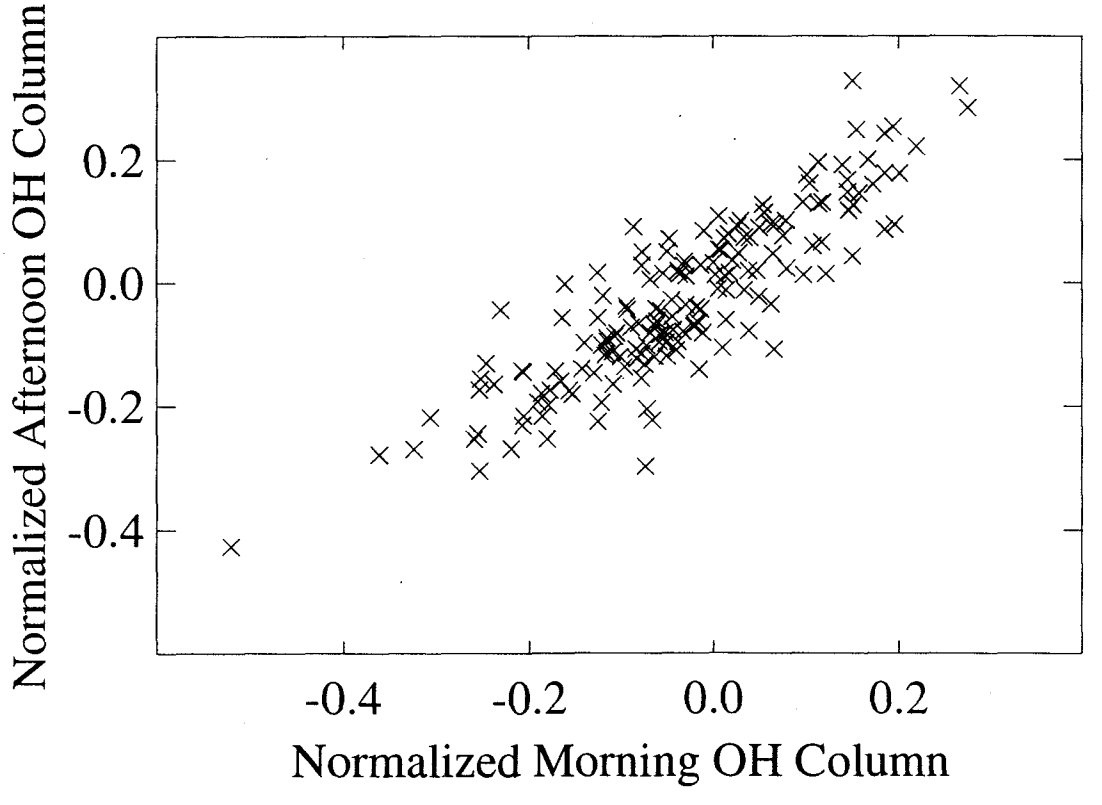
Normalized Afternoon OH Column
0.2
0.0
-0.2
-0.4
-0.4
-0.2
0.0
0.2
Normalized Morning OH Column

Figure 7

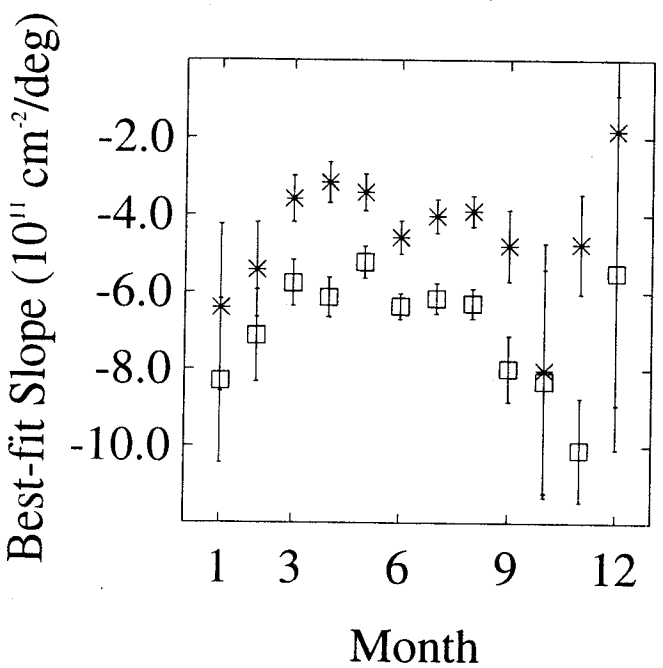

Figure 8

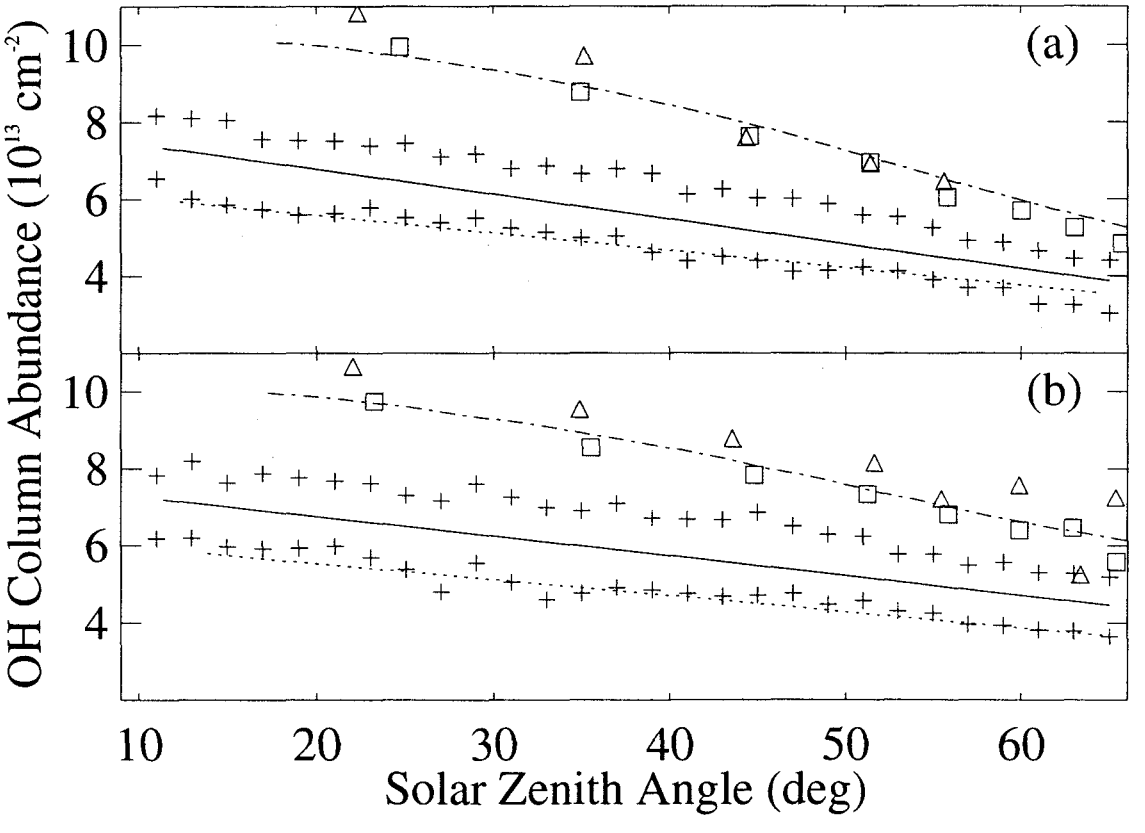
OH Column Abundance (10^{13} cm^{-2})
10
8
6
4
(a)
(b)
10
20
30
40
50
60
Solar Zenith Angle (deg)

Figure 9

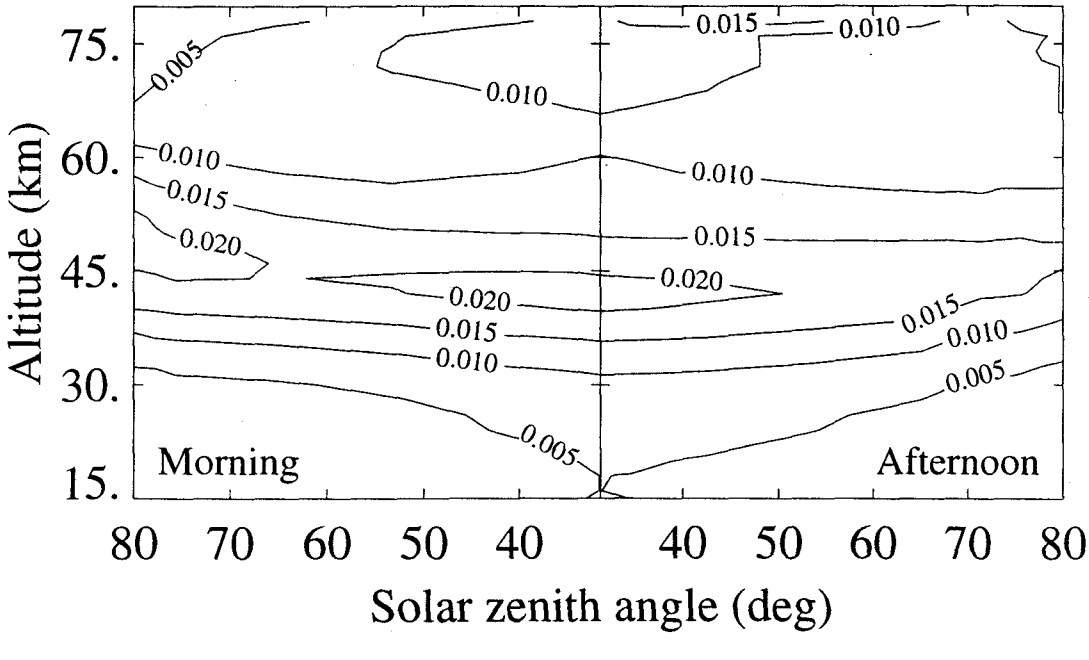
75.
60.
45.
30.
15.
Altitude (km)
0.005
0.010
0.015
0.020
Morning
Afternoon
80 70 60 50 40
40 50 60 70 80
Solar zenith angle (deg)

Figure 10

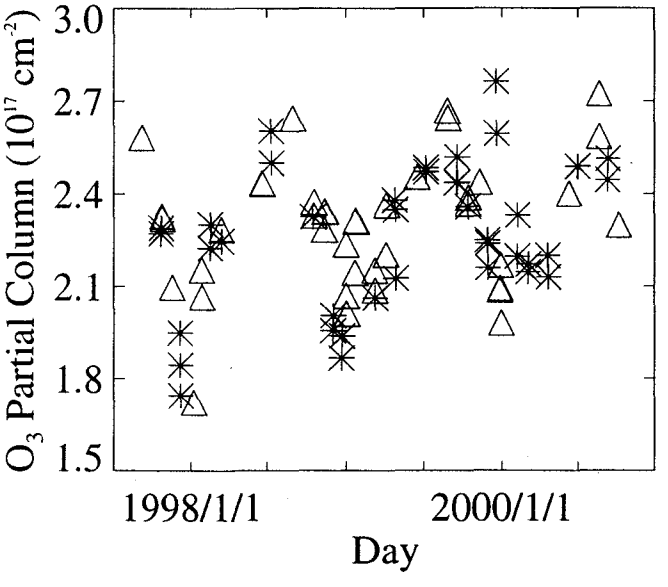

Figure 11

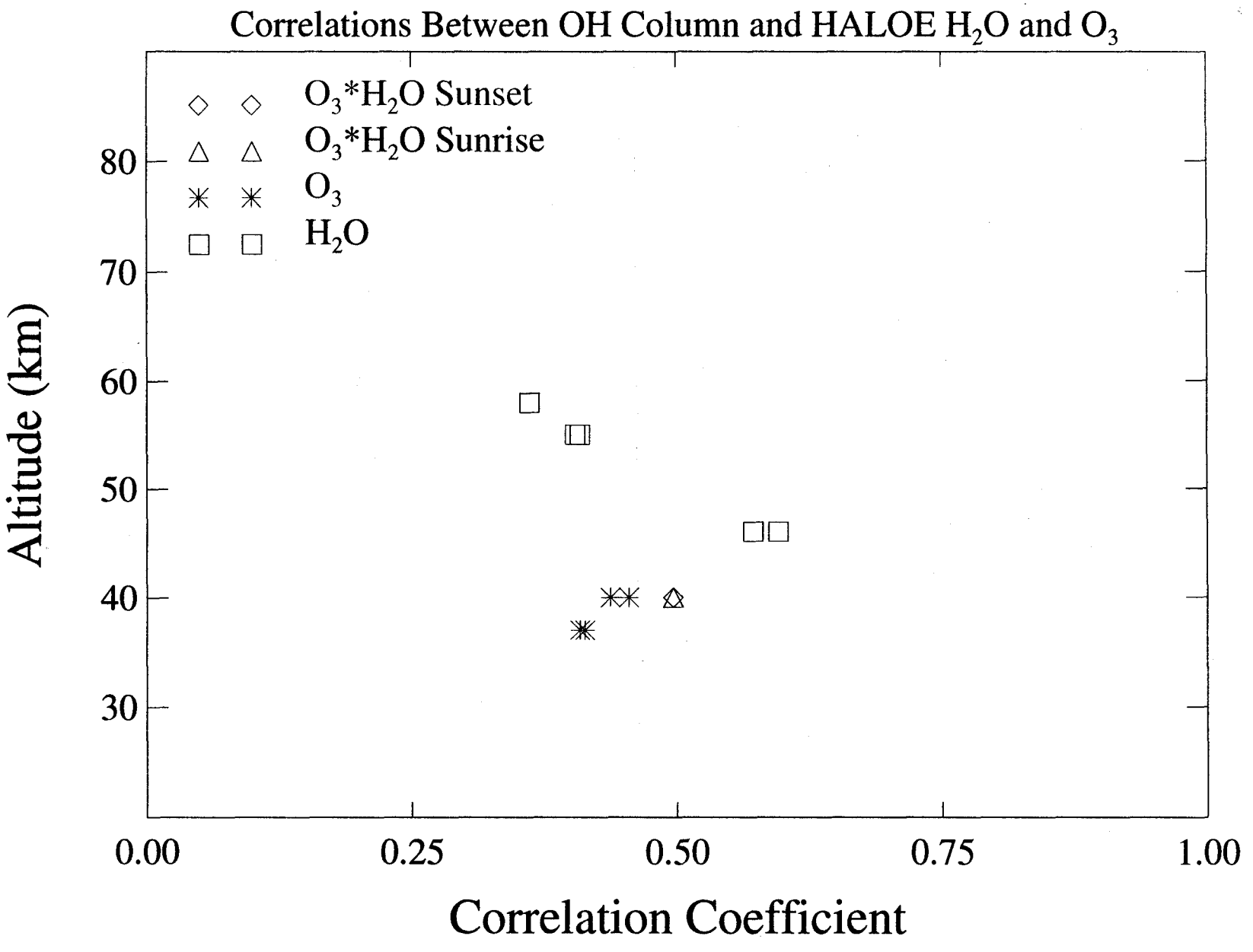
Correlations Between OH Column and HALOE H_2O and O_3
O_3*H_2O Sunset
O_3*H_2O Sunrise
O_3
H_2O
Altitude (km)
80
70
60
50
40
30
0.00
0.25
0.50
0.75
1.00
Correlation Coefficient

Figure 12

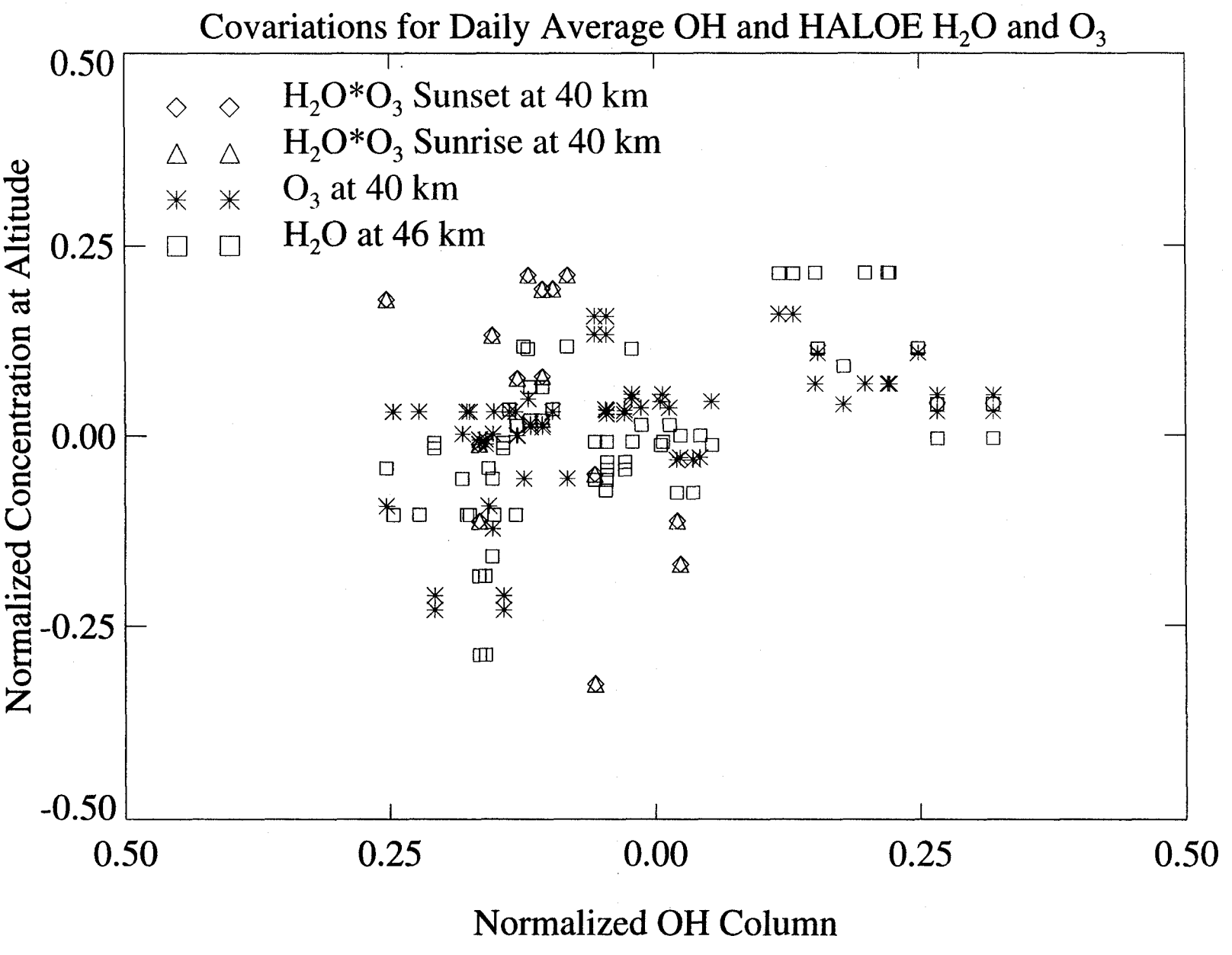
Covariations for Daily Average OH and HALOE H_2O and O_3
H_2O*O_3 Sunset at 40 km
H_2O*O_3 Sunrise at 40 km
O_3 at 40 km
H_2O at 46 km
0.50
0.25
0.00
-0.25
-0.50
0.50
0.25
0.00
0.25
0.50
Normalized Concentration at Altitude
Normalized OH Column

Figure 13

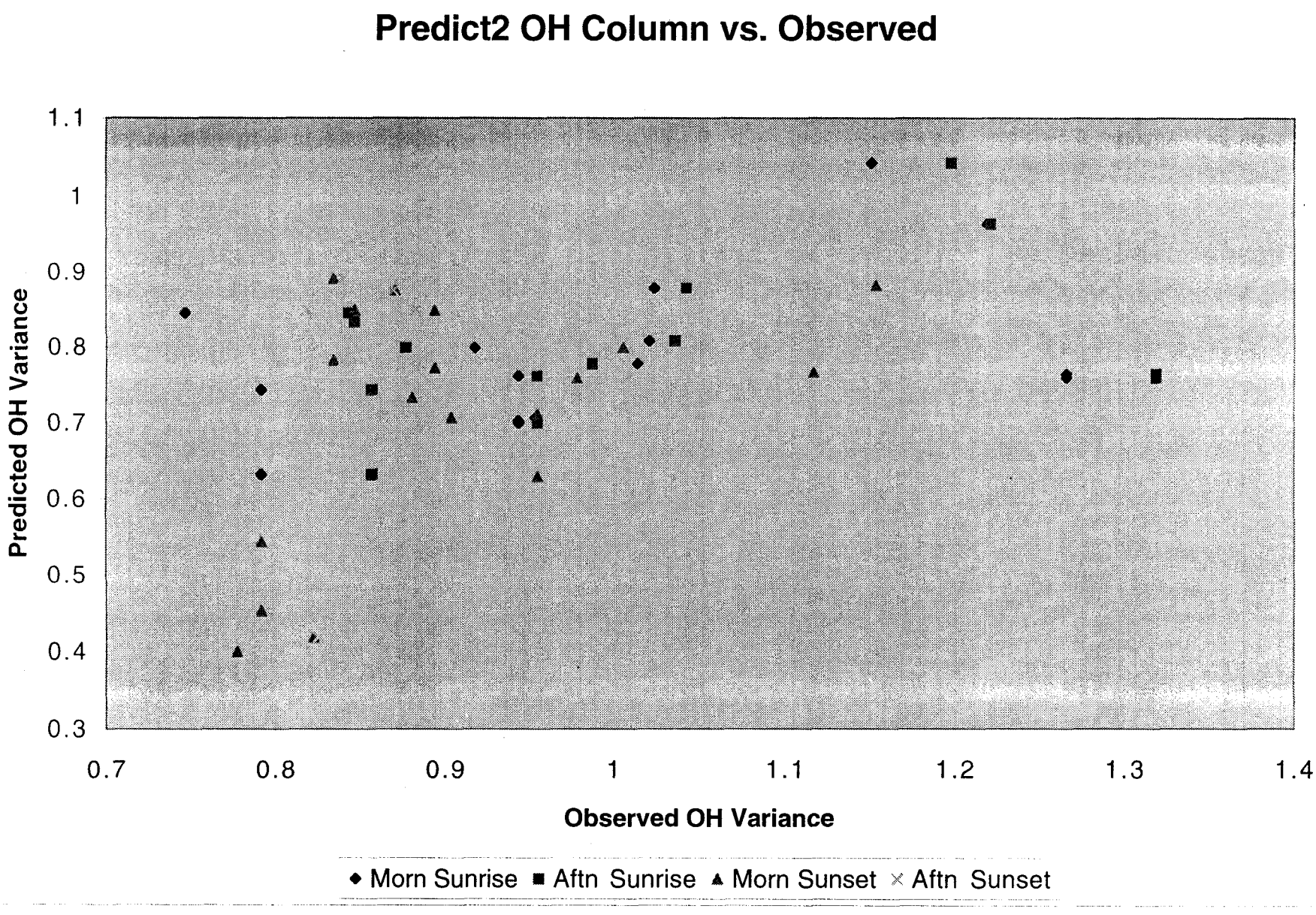
Predict2 OH Column vs. Observed
Predicted OH Variance
1.1
1
0.9
0.8
0.7
0.6
0.5
0.4
0.3
0.7
0.8
0.9
1
1.1
1.2
1.3
1.4
Observed OH Variance
Morn Sunrise
Aftn Sunrise
Morn Sunset
Aftn Sunset